

Editor
Júlio Manuel R.S. Teixeira



Computer Methods in Biomechanics and Biomedical Engineering: Imaging & Visualization

ISSN: (Print) (Online) Journal homepage: www.tandfonline.com/journals/tciv20

A CFD-based framework to evaluate surgical alternatives in cerebral aneurysms

Martina Schena, Federica Testa, Michela Bozzetto, Andrea Remuzzi, Luigi A. A. Lanterna & Ettore Lanzarone


To cite this article: Martina Schena, Federica Testa, Michela Bozzetto, Andrea Remuzzi, Luigi A. A. Lanterna & Ettore Lanzarone (07 Mar 2024): A CFD-based framework to evaluate surgical alternatives in cerebral aneurysms, *Computer Methods in Biomechanics and Biomedical Engineering: Imaging & Visualization*, DOI: [10.1080/21681163.2024.2325351](https://doi.org/10.1080/21681163.2024.2325351)

To link to this article: <https://doi.org/10.1080/21681163.2024.2325351>



© 2024 The Author(s). Published by Informa UK Limited, trading as Taylor & Francis Group.




View supplementary material 



Published online: 07 Mar 2024.



Submit your article to this journal 



View related articles 



View Crossmark data 

A CFD-based framework to evaluate surgical alternatives in cerebral aneurysms

Martina Schena^a, Federica Testa^a, Michela Bozzetto ^b, Andrea Remuzzi ^a, Luigi A. A. Lanterna ^c
and Ettore Lanzarone ^a

^aDepartment of Management, Information and Production Engineering, University of Bergamo, Dalmine, Italy; ^bLaboratory of Medical Imaging, Istituto di Ricerche Farmacologiche Mario Negri IRCCS, Ranica, Italy; ^cNeurosurgery Division, Papa Giovanni XXIII Hospital, Bergamo, Italy

ABSTRACT

Computational Fluid Dynamic (CFD) simulations on patient-specific geometries may guide the choice between alternative surgical interventions, especially in the case on non-conventional treatments. We propose and formalise a CFD-based framework to evaluate alternative surgical interventions. It provides surgeons with the CFD analyses of different surgical options, so that they may decide the best strategy based on quantitative haemodynamic parameters for each surgical alternative. The proposed framework is largely automatised and, when it necessarily requires the intervention of a human operator due to the patient-specific nature, this intervention is well-formalised to reduce inter-operator variability and guarantee reproducibility. To provide preliminary evidence on the effectiveness of the framework, we present its application to complex Intracranial Aneurysms (IAs), which involve less than 5% of brain aneurysms, but are usually at a high risk of rupture and often show unexpected response to therapy. Complex IAs include aneurysms that cannot be treated with conventional therapies, such as neck clipping, sac coiling or stenting, while instead their treatment requires the sacrifice of the parent artery. In particular, we refer to a giant cavernous sinus aneurysm inside the left internal carotid artery. Results show the ability of the framework to provide haemodynamic quantitative evaluations, which can be useful additional information for the neurosurgeon towards optimal surgical planning.

ARTICLE HISTORY

Received 2 June 2023
Accepted 24 February 2024

KEYWORDS

Complex intracranial aneurysms; standardized framework; patient-specific hemodynamics; computational fluid dynamics

1. Introduction

Accurate haemodynamic analyses of the alternative surgeries to treat aneurysms are fundamental to better design flow deviations in all cases where common endovascular treatments may not be beneficial (Zhao et al. 2018). A widely considered strategy for these cases is the so-called *hunterian ligation*, whose rationale is to occlude the aneurysm without directly intervening on it. It consists of an occlusion of the parent artery proximal to the aneurysm, causing the aneurysm to thrombose. Then, regional circulation is restored via bypass (Ishishita et al. 2014; Walcott et al. 2016; Wessels et al. 2021; Rutledge et al. 2022).


Computational Fluid Dynamics (CFD) can support decision making in these treatments, by providing flow, pressure and Wall Shear Stress (WSS) in ideal or patient-specific geometries, and information on the complications that can result from surgery, such as ischaemia (Pekkan et al. 2008; Botti et al. 2018). CFD does not involve invasive procedures, but only requires Computed Tomography Angiography (CTA) or Magnetic Resonance (MR) images of the patient's vascular district. It was applied to analyse aneurysm characteristics and progression. But also, CFD can provide a description of the postoperative haemodynamic conditions of any alternative surgical treatment, to compare the treatments with each other. Indeed, the main benefit of using CFD is to quantify haemodynamic variables before and after surgery,

allowing a more complete evaluation of surgical alternatives when two or more are technically possible and none is preferable *a priori*. Therefore, the surgeon can plan the intervention based not only on the patient's anatomical images and the technical complexity of the surgery, but also on a quantitative prediction of the effect of the intervention on haemodynamics. Although some consequences of a specific surgical procedure in terms of haemodynamic changes could be predicted qualitatively, the quantification and formal representation of these changes can add important information.

In this context, clinical cases must be assessed individually, but this does not preclude defining a general framework valid for all patients. Indeed, recent discussions highlighted that standardisation of pre-simulation and post-simulation steps are crucial to provide reliable CFD results (Berg et al. 2019). To this end, we propose a CFD-based framework for evaluating alternative surgical interventions.

Preliminary evidence on the effectiveness of the proposed framework is provided through application to a complex Intracranial Aneurysm (IA), i.e., a particularly complex Internal Carotid Artery (ICA) aneurysm. Complex IAs refer, by definition, to aneurysms that cannot be treated with conventional therapies, such as neck clipping, sac coiling or stenting, while instead their treatment requires the sacrifice of the parent artery

CONTACT Ettore Lanzarone  ettore.lanzarone@unibg.it  Department of Management, Information and Production Engineering, University of Bergamo, Dalmine, BG, Italy

 Supplemental data for this article can be accessed online at <https://doi.org/10.1080/21681163.2024.2325351>

© 2024 The Author(s). Published by Informa UK Limited, trading as Taylor & Francis Group.

This is an Open Access article distributed under the terms of the Creative Commons Attribution-NonCommercial License (<http://creativecommons.org/licenses/by-nc/4.0/>), which permits unrestricted non-commercial use, distribution, and reproduction in any medium, provided the original work is properly cited. The terms on which this article has been published allow the posting of the Accepted Manuscript in a repository by the author(s) or with their consent.

(Andaluz and Zuccarello 2011; Hofman et al. 2018; Pescatori et al. 2022). These aneurysms are typically fusiform or giant (particularly if they are thrombosed), calcified, in difficult and deep locations, and with branches arising from the aneurysm itself. Complex IAs involve less than 5% of brain aneurysms (Beecher and Welch 2017), but are highly risky in terms of unexpected evolution and therapy response, and may rupture and bleed.

2. Materials and methods

The proposed framework defines a general approach to provide neurosurgeons with CFD analyses of different surgical options for complex IAs.

2.1. Structure of the framework

The framework has a modular structure, as shown in Figure 1. First, patient-specific images and information about the characteristics of the IA, which are the first two inputs to the framework, are used to generate the three-dimensional virtual geometry. In case, some secondary arteries are not visible from the images but crucial for CFD simulations, they are added by including a sensitivity analysis to adopt the best assumptions for the unknown diameters. The resulting alternative geometries represent the baseline preoperative case and the CFD simulation is performed for all of them. The neurosurgeon evaluates CFD results in terms of flows, pressure and WSS in the alternative geometries. Then, as a third input to the

framework, the neurosurgeon proposes a set of alternative flow-altering surgical procedures, by adapting the guidelines to the specific patient according to similar cases in the literature, his/her expertise, and the preoperative CFD results. Alternative procedures may include, e.g., different clipping positions, trapping strategies, bypass inclusions, and combinations thereof. Each preoperative geometry is modified to represent the different surgical procedures, and the CFD simulation is then run on all the obtained geometries. A score is assigned to each CFD simulation, combining also some clinical information such as the adequacy of the perfusion in downstream vessels, the risk for the patient, the technical difficulties of the procedure, and the expected success of the intervention. The neurosurgeon analyses the scores and either ranks the alternatives and decides on the surgical treatment to perform, or asks to simulate further treatments.

Given its modular structure, the framework is flexible and easily receptive to extensions. Moreover, it is largely automated and, when it requires a human operator due to its patient-specific nature, the intervention is well-formalised to reduce inter-operator variability.

The time needed by a suitably trained and expert technician to apply the framework to a case of medium complexity as the one presented below, from the clinical case study to the achievement of results, is about 55 hours, of which 17 are dedicated to run all the alternative CFD simulations. Simulations were run on a Microsoft Windows machine with CPU Intel Core i5 10210U and 12 GB of installed RAM.

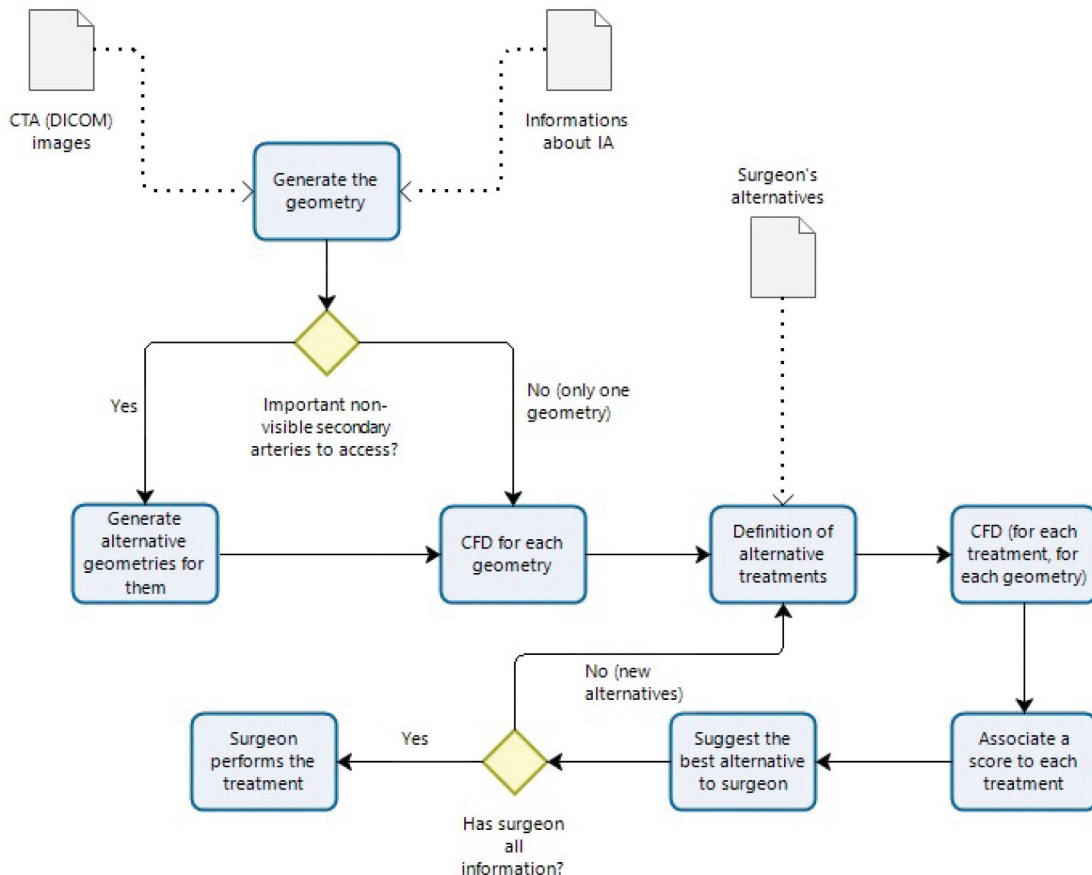


Figure 1. Representation of the proposed CFD-based framework.

2.2. Sensitivity versus alternative geometries

Despite small-calibre secondary arteries are poorly visible from CTA images, these vessels must remain open to avoid ischaemic complications when the flow is diverted. The best option is to explore in advance a range of possibilities that may occur when opening the skull, i.e., to include the non-segmentable perforating branches assigning them at least 4 arbitrary diameters values within a reference range from the literature (Saeki and Rhoton 1977). In case of several vessels, all combinations of diameters are considered.

Any surgical treatment is compared with the baseline under the same combination of diameters. Then, it is analysed whether the comparison result is stable and the decision remains the same as the diameters change. In case of variations, the neurosurgeon nevertheless receives suggestions on how to act depending on the unknown variables. Then, he/she makes assumptions about the actual diameters or observes them while performing the surgery.

2.3. Clips and bypasses for surgical treatments

Virtual clips and bypasses are the key elements that simulate the surgical treatments in the baseline geometries.

A clip is inserted through a clipping box followed by a capping of the open boundaries. The box is inserted across the artery perpendicular to the vessel centerline. After cutting, the openings are closed by a smooth-capping filter. Flat caps are applied, and the vessel portion being cut is about 1 mm long. An example is shown in Figure 2(a,b).

Bypass placement consists of inserting an additional segment into the network, i.e., a tubular structure of tailored length, radius and curvature, by means of the *Active Tubes*

algorithm (Manini 2013). It allows drawing a pipeline by inserting spheres in the image, whose diameter represents the diameter of the vessel at that point (Figure 2(c,d)).

2.4. CFD-aided decision making

The surgical treatments are compared under the alternative geometries for secondary vessels, if any, to establish the most effective treatment in terms of aneurysm healing and preservation of blood vessels. Several factors must be considered when comparing and scoring, the most important of which are classified in Figure 3.

As for network reaction, velocity streamlines allow to identify low-flow areas, vortexes and recirculation. Poorly or non-perfused secondary arteries are a symptom of blood stagnation and thrombosis, resulting in artery occlusion and brain damage or death. Finally, the absence of flow should be alarming when the perforating arteries lie after a clip. Pressure maps highlight changes in flow direction, together with an increased WSS when flows coming from many directions converge in a point. Pressure drops should not increase after surgery to avoid the risk of wall rupture, making the solution with lowest drop between inlets and outlets preferable.

The same maps assess the multi-arterial involvement in the presence of several tributary arteries that feed the IA, when the application of a clip redistributes the flow in the network. Velocity streamline and isosurface maps can be studied to understand the most effective inlet closures when placing the clips. It must be ensured that, if one or more of the branches are closed, the downstream blood supply remains adequate. Also, to avoid serious damage to the perforating arteries, the best solution is to reduce the flow in a safe way, i.e., preserving

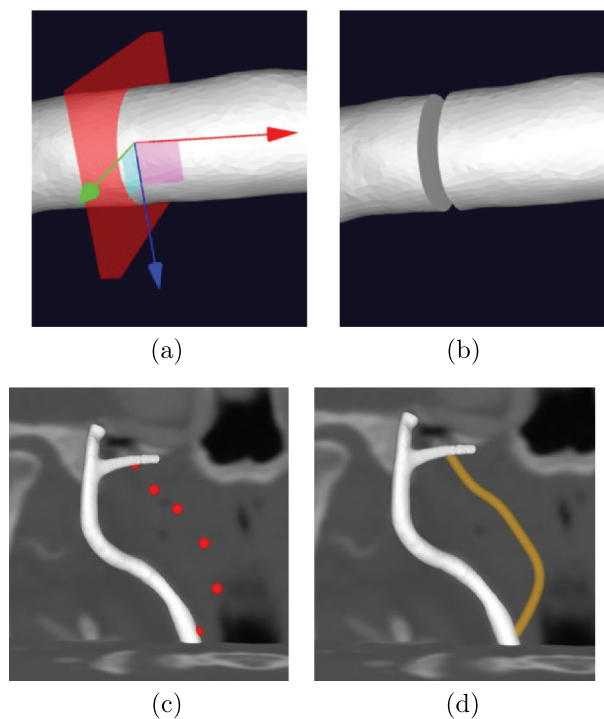


Figure 2. Cut (a) and capping of extremities (b) to simulate a clip. Bypass placement: insertion of spheres that outline the vessel (c) and resulting bypass vessel (d).

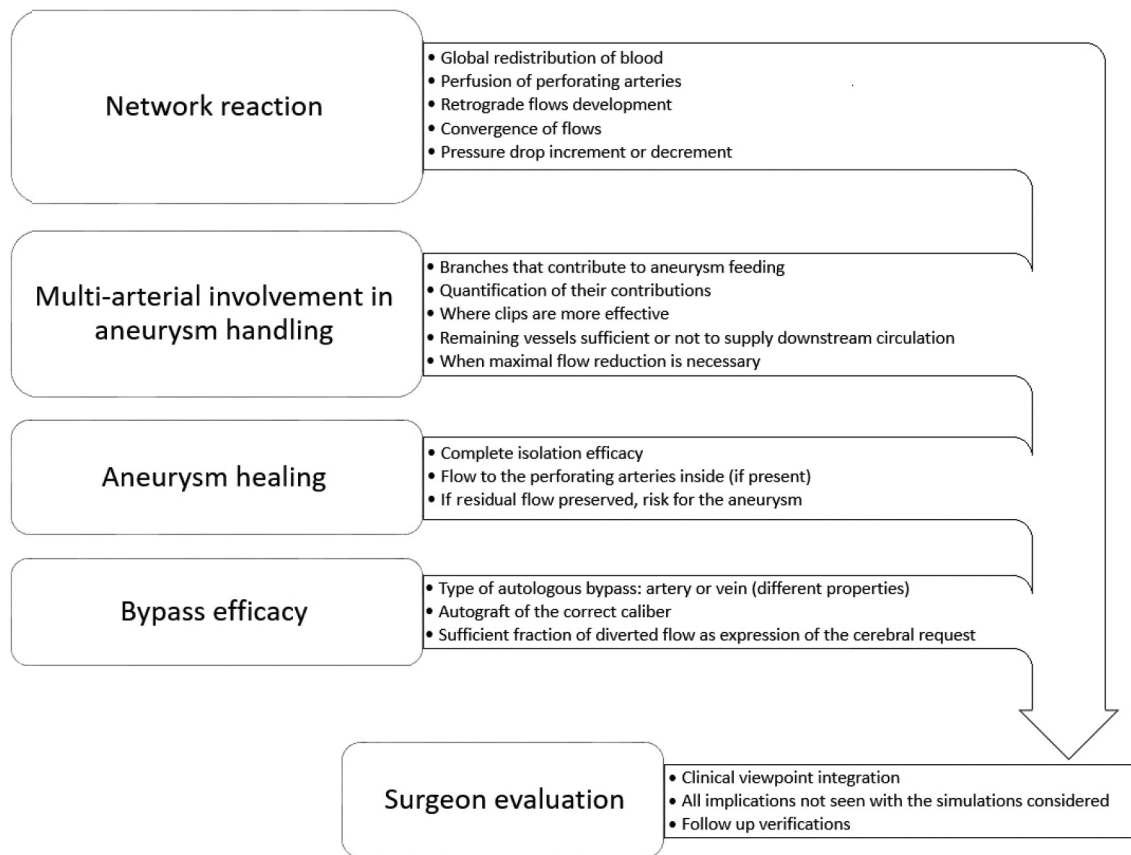


Figure 3. Factors to compare the surgical alternatives.

residual flow to the smaller vessels and preventing the aneurysm from growing thanks to the low flow.

As for aneurysm healing, in the presence of small arteries fed by the aneurysmal area, the blood flow in the aneurysm cannot be interrupted. Otherwise, if the vessel segment to treat has no downstream arteries to supply, the aneurysm can be simply isolated through clips to promote the formation of a thrombus.

Concerning bypass efficacy, the aim is to divert as much flow into the graft with respect to the parent artery. The calibre of the implanted vessel should be similar to that of the bypassed artery. High pressure drops, WSSs and velocity values in the bypass indicate that it is proportionate to the demand, which ensures longer bypass life.

2.5. Framework steps

The whole framework consists of the following steps:

2.5.1. Segmentation

It consists of extracting the voxels that make up the walls of the vessels to be included in the 3D model. It includes an initialisation followed by a refinement. The initialisation is performed with the *Colliding Fronts* method for vessels with cylindrical shape, and with the *Fast Marching* method for saccular aneurysms. Moreover, vessels difficult to identify are included manually with the *Active Tubes* algorithm.

The refinement is automatic, starting from the initialised geometry. The reconstruction of large networks is carried out in separate chunks, which are then merged into a single and cohesive model. A general smoothing is finally applied to the whole surface, using standard approaches like the low-pass Laplacian smoothing and the Taubin smoothing. In our tool, the segmentation step and the general smoothing are performed with the VMTK libraries (<https://www.vmtk.org>) and the associated visualisation software VMTKLab (Orobix, Italy). In addition, a local smoothing is performed using MeshMixer (Autodesk, CA, US); in this case, the entire surface is further smoothed at the end with a general smoothing.

2.5.2. Surface mesh

A triangular surface mesh is generated through the *Marching Cubes* algorithm. Moreover, a manual procedure is carried out to fix possible inaccuracies in the surface mesh: the compromised parts of the mesh (holes, non-manifold regions and small-component areas) are fixed with MeshMixer (Autodesk, CA, US).

2.5.3. Surface pre-processing

The surface model is processed to generate a mesh suitable for the CFD analysis. This step includes four subsequent activities, which can be automatically performed using VMTKLab: *clipping*, *smooth capping*, *flow extensions addition*, and *surface remeshing*.

2.5.4. Volume meshing

The volume is filled with a combination of tetrahedral, pyramidal, hexahedral and prismatic elements. This step is performed using the ANSYS Fluent solver (ANSYS Inc., PA, US), which is based on the finite volume method. To ensure the reliability of the results, a mesh density sensitivity analysis is included in the tool. It consists of running the CFD on the same geometry with increasing densities and comparing the results. When the results in terms of WSS and velocity are stable, a sufficient density is reached. Then, the proper setting with the least number of elements is preferable to limit complexity and computational time.

2.5.5. Computational fluid dynamics

CFD is performed by means of the ANSYS Fluent solver. In the CFD simulations, blood is assumed to be homogeneous and

incompressible, the flow is assumed laminar, and the *Carreau non-Newtonian* model is used for the viscosity. Accordingly, the fluid dynamics problem is modelled by coupled Navier–Stokes equations. Time is steady and the artery wall motion is set to stationary, to specify a fixed wall.

Further technical details of each step are reported in the Online Supplementary Materials.

3. Results

3.1. Test case

We applied the proposed framework to study a giant cavernous sinus aneurysm in the C3 portion of the left ICA (within the cavernous sinus to the passage through the dura mater), whose shape is approximately a sphere with diameter of 25 mm (Figure 4).

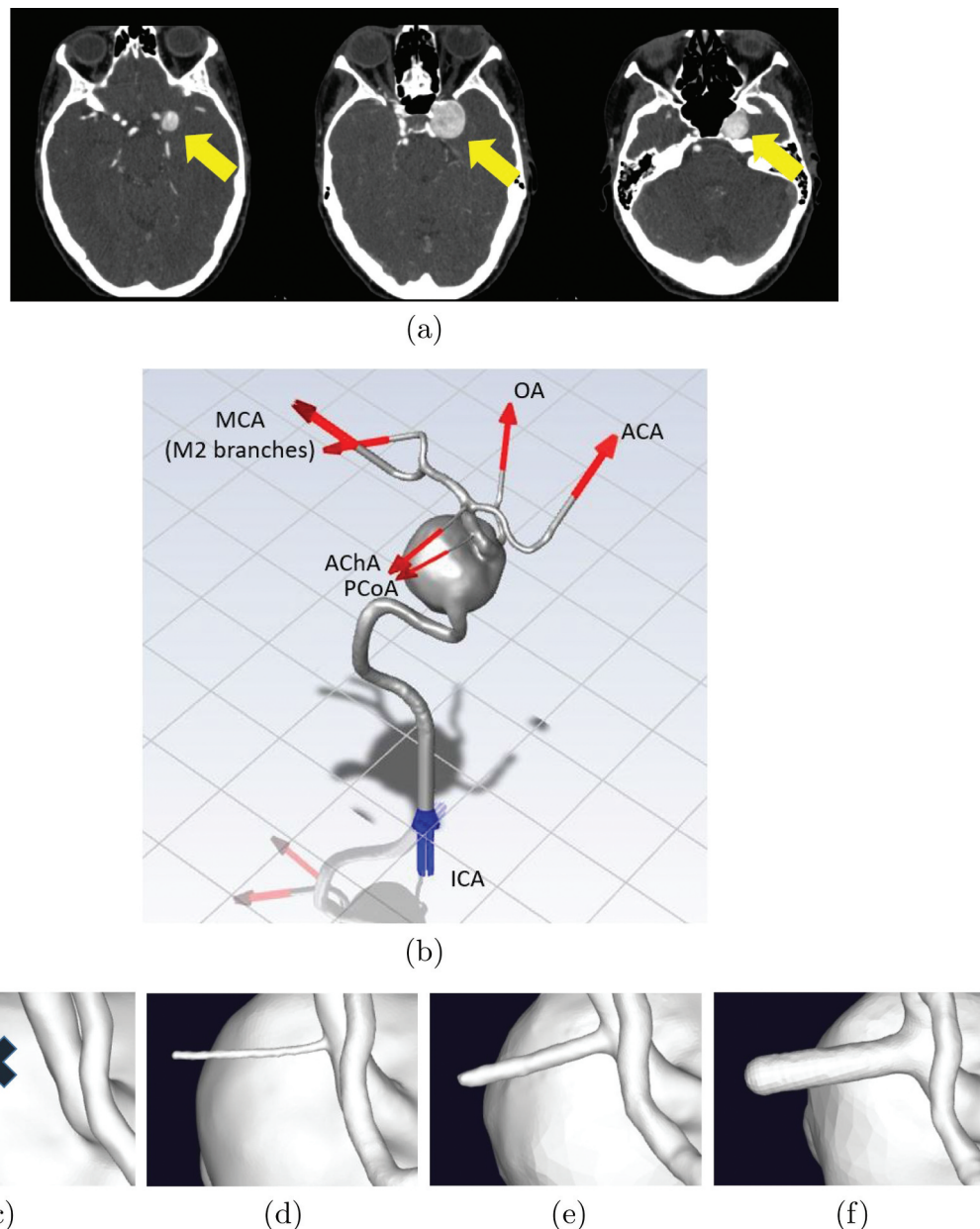


Figure 4. Location of the aneurysm in transverse CTA images at different height (a). Aneurysm reconstructed geometry with involved vessels, inlet through the ICA, and outlets through the two MCA branches, the OA, the ACA, the AChA and the PCoA (b). PCoA scenarios: S_0 (c), S_m (d), S_a (e), S_M (f).

The blood flow enters through the left ICA and exits through the two branches of the Middle Cerebral Artery (MCA), the Ophthalmic Artery (OA), the Anterior Cerebral Artery (ACA), the Anterior Choroidal Artery (AChA) and the Posterior Communicating Artery (PCoA), as illustrated in Figure 4b. An average inflow rate into the left ICA of 264 mL/min (Zhao et al. 2007; Wei et al. 2019) was assumed; with a diameter of 4.03 mm , it corresponds to a velocity of 0.35 m/s in all CFD simulations (Grant et al. 2003; Özdemir et al. 2006). In addition, traction-free condition was set at the exits, which is a common assumption also reported in recent works.

The patient, enrolled at the Papa Giovanni XXIII Hospital in Bergamo, Italy, signed an informed consent agreement which complied with Italian legislation (Codex on Privacy, D. Lgs. 30 giugno 2003, n. 196).

The PCoA was poorly visible in the CTA images. Therefore, we tested four cases (Figures 4c-f): absence of PCoA (S_0), minimum diameter equal to 0.3 mm (S_m), average diameter equal to 1.3 mm (S_a), and maximum diameter equal to 3.1 mm (S_M).

3.2. Surgical solutions

Three surgical solutions were identified (Figure 5):

- Proximal clipping (PC), which consists of a closure at the neck upstream of the aneurysm. It is the most common and safe technique because the ICA is easily accessible and the risk of bleeding is low. In addition, the OA can draw the flow distally from the bypass, ensuring a low retrograde flow.
- Distal clipping (DC), which consists of a closure of the ICA downstream of the aneurysm. It has higher risk of bleeding and longer healing rate than PC (Wessels et al. 2021). Moreover, the AChA and the PCoA, the last two arteries to be perfused by the bypass, may be at risk of occlusion due to lack of retrograde flow.

- Trapping of C3 portion (TC3), which is a combination of the other techniques. Two clips are placed at the extremes of the aneurysm to completely isolate it, since no vital perforating arteries are present in the aneurysm region and the OA is compensated by the External Carotid Artery (ECA). No retrograde flow develops in the aneurysm, guaranteeing rapid thrombosis, but the risk of AChA ischaemic stroke is very high because of the distal clip.

All interventions require a high-flow bypass (Ishishita et al. 2014) that diverts blood from the cervical portion of the ICA to the inferior M2 segment of the MCA after it bifurcates. It is performed by resecting part of the radial artery, which has proper wall properties and size to replace the ICA, i.e., average diameter of 2.3 mm (Ashraf et al. 2010).

3.3. CFD outcomes

The maximum pressure drops between any pair of points in the domain are reported in Table 1, while the pressure drop maps in Figure 6 for S_a and in the Online Supplementary Materials for the other scenarios. In general, the obtained pressure drops are in line with the literature (Alnæs et al. 2007; Müller et al. 2012). Higher pressure drops were observed with PC and TC3 than with DC, because the flow was completely diverted from the bypass and the ICA was clipped proximal to the aneurysm with PC and TC3, while the flow was distributed between the bypass and the ICA with DC. Moreover, all drops were higher than in the pathological preoperative case due to the clips. When varying the PCoA diameter, the highest differences in pressure drop with respect to the preoperative case were observed for S_M , while the lowest differences for S_m or S_a depending on the case. Comparing preoperative and surgical cases, the pressure drops in the bypass and in the segment C2 of the ICA were greater with PC than with TC3 for S_0 and S_M , while the reverse occurred with S_m and S_a . Anyway, in all PCoA scenarios of PC

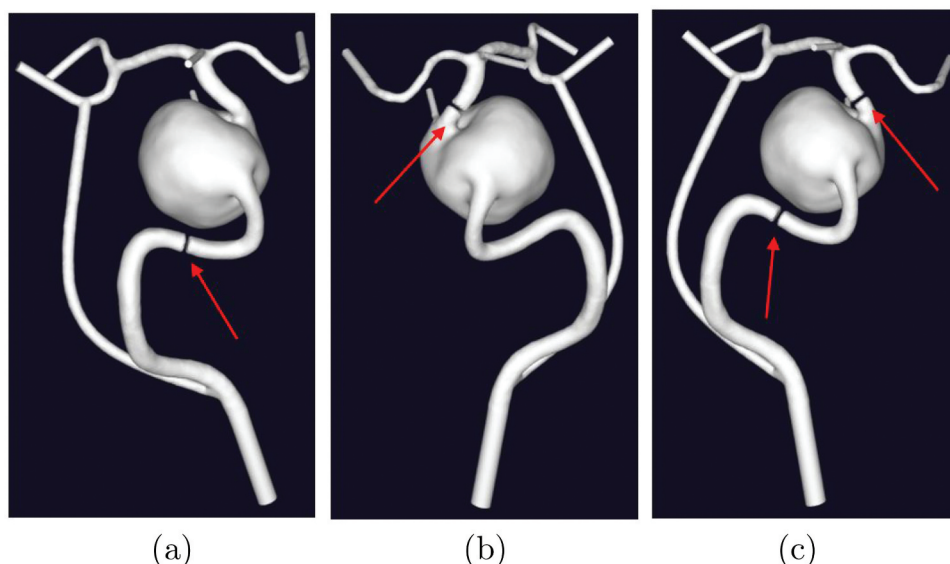


Figure 5. Representation of different surgical solutions (geometry without PCoA): PC (a); DC (b); TC3 (c). Red arrows indicate the clipping sites.

Table 1. Pressures drops corresponding to the different surgical options.

	Pressure drops [$10^3 Pa$]			
	Preoper	PC	DC	TC3
S_0	2.49	6.87	4.14	6.53
S_m	2.35	5.29	3.73	5.52
S_a	2.26	5.24	3.35	5.47
S_M	1.19	4.49	2.80	4.08

and TC3, they were closer together, while with DC the pressure drop was noticeably lower. The aneurysm was excluded from the circulation with TC3. In the other cases, the pressure inside the aneurysm was lower than that in the preoperative case with PC and higher with DC. This consideration was stable when varying the PCoA diameter.

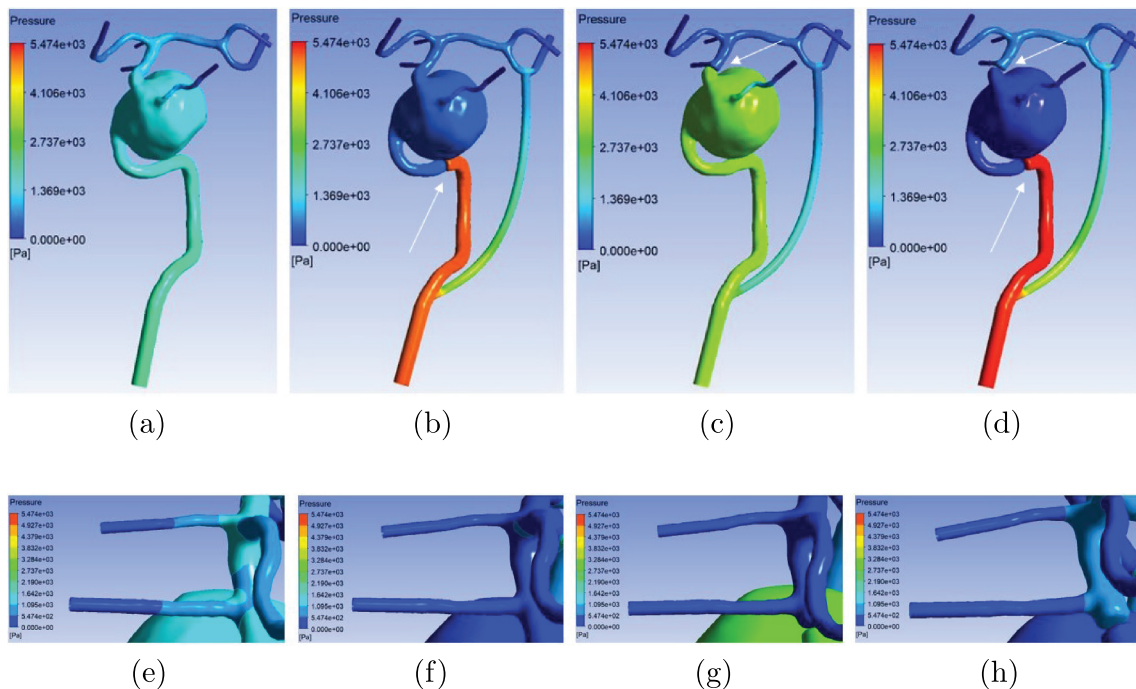
The WSSs at the neck of the aneurysm and in the C4 portion of the ICA (between the subarachnoid space and the bifurcation into the anterior and middle cerebral arteries) are reported in Table 2, while the pressure maps in Figure 7 for S_a and in the Online Supplementary Materials for the other scenarios. All surgeries lowered the WSS in the ICA and halved the values in the curvatures of the C2 and C3 portions (in the middle of the carotid canal), at the expense of the bypass. In the preoperative case, a moderate WSS was observed at the entrance of the aneurysm where the ICA enlarged, while all surgical solutions made the WSS equal to zero. As for the OA, it remained isolated together with the aneurysm with TC3 and, therefore, it was not subject to WSS at all. With a proximal clip, a little WSS increase was observed in the OA with respect to the preoperative case, which may be due to the sudden narrowing of the perforating vessel. The AChA was subject to lower WSS after surgery. Specifically, the lowest reduction was observed with TC3, followed by PC, and the greatest reduction was observed with DC. The same phenomenon occurred for the PCoA, located below.

Table 2. WSSs.

	Preoper	PC	DC	TC3
WSS at the neck of the aneurysm [Pa]				
S_0	6.42	$1.22 \cdot 10^{-3}$	1.65	$3.35 \cdot 10^{-17}$
S_m	7.02	$1.58 \cdot 10^{-3}$	1.05	$2.40 \cdot 10^{-19}$
S_a	14.49	$1.66 \cdot 10^{-3}$	1.15	$5.29 \cdot 10^{-17}$
S_M	5.24	$1.81 \cdot 10^{-4}$	0.84	$5.61 \cdot 10^{-17}$
WSS in the C4 portion of ICA [Pa]				
S_0	2.57	0.25	$6.51 \cdot 10^{-3}$	0.039
S_m	2.84	0.56	0.51	0.11
S_a	2.21	0.54	0.33	0.36
S_M	0.68	1.64	1.12	1.51

A remarkable reduction of WSS at the neck of the aneurysm was very observed with PC, with a decrease of more than 99.9% in all PCoA alternatives. With DC, the reduction was less significant (between 75% and 92%, with the smallest reduction for S_0) due to the blood that continued to arrive to the aneurysm. Finally, TC3 made the WSS in the aneurysm equal to zero. Clip positioning also influenced the WSS in the C4 segment of the ICA, between the origin of two perforating arteries. In this position, the reduction with respect to the preoperative case was smaller when the clip preceded the aneurysm with respect to when the clip was downstream the aneurysm, and TC3 showed an intermediate decrement. For the AChA no trends were observed for any surgery. The WSS decrease in the AChA with respect to the preoperative case seemed to be stable for the different scenarios and surgical alternatives, except for S_M which showed a smaller deviation with PC and TC3.

While varying the PCoA diameter, there were no differences regarding the proximal ICA and the aneurysm; only the OA with DC in scenario S_M showed an increase in WSS higher than in the other three scenarios. As a consequence, WSS results showed no particular differences with respect to the PCoA diameter

**Figure 6.** Anterior (a–d) and right side (e–h) view of pressure drop maps for S_0 ; preoperative (a,e); PC (b,f); DC (c,g); TC3 (d,h). Clips positions in PC, DC and TC3 are denoted by white arrows.

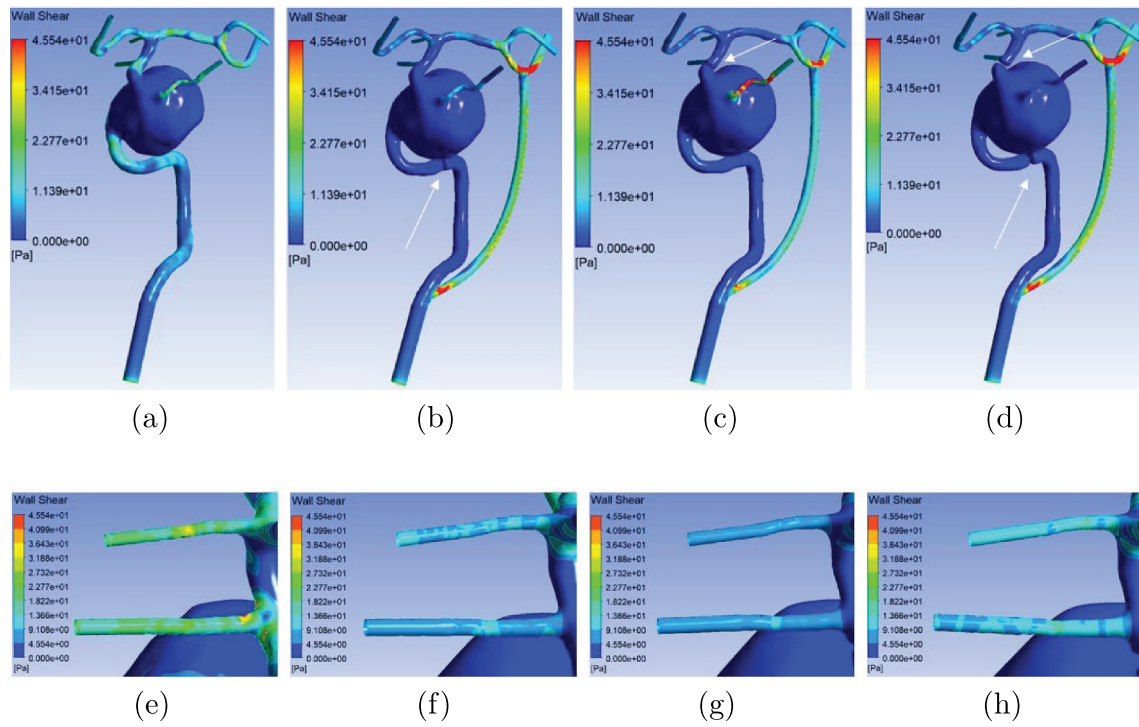


Figure 7. Anterior and right side view of WSS maps for S_a (subfigures and arrows as in Figure 6).

when comparing the treatment alternatives, with the exception of S_M .

We finally analyse the velocities, whose streamline maps are reported in Figure 8 for S_a and in the Online Supplementary Materials for the other scenarios. Although the streamlines

provide qualitative information, their knowledge gave us insight into velocity distributions, which can be coupled with the other information on pressures and WSS discussed earlier. Only a few spots of high velocities occurred in the bypass and the OA, in agreement with the WSS results, while most of the

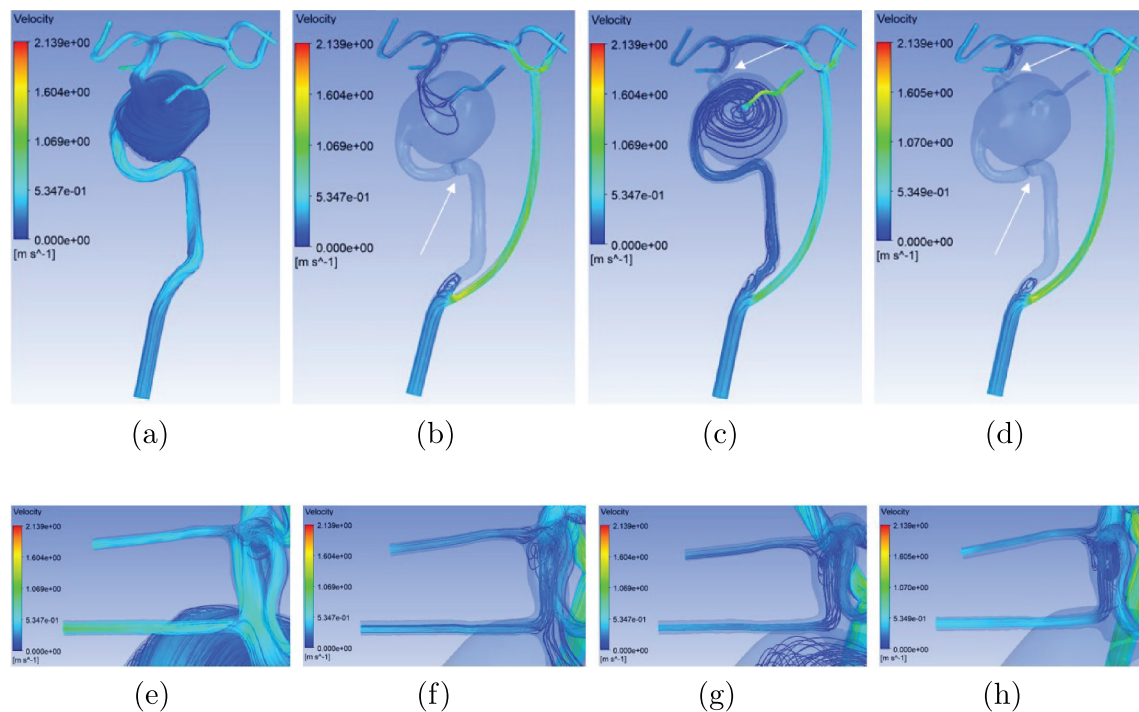


Figure 8. Anterior and right side view of velocity streamlines for S_a (subfigures and arrows as in Figure 6).

domain was characterized by velocity values that at most doubled the inlet velocity. With PC and TC3, all flow was diverted into the bypass and a low velocity recirculation formed close to the bypass grafting. Moreover, blood was able to reach the upper part of the network via the bypass, supplying the MCA and the ACA; with PC, also the perforating arteries and the ophthalmic region were perfused in a retrograde manner. With DC, the flow was distributed between the bypass and the ICA, which remained pervious; therefore, it reached the aneurysm where circular trajectories originated. Moving at low velocity, they favoured blood stagnation and, consequently, thrombosis in the weakened part of the vessel. All the surgeries reduced the flow in the aneurysm: DC caused the non-diverted flow portion to come directly from the ICA; PC blocked the direct flow and that coming retrograde was much less than with DC; TC3 completely isolated the aneurysm. As a result, the OA was affected by these

flow alterations: there was no flow with TC3, but this did not represent a risk as the vessel had the ECA as a second tributary; the OA was able to attract a minimal flow with PC, less consistent and slower than with DC. Only in the latter case the velocity was higher than in the preoperative one. According to pressure and WSS maps, velocity was higher in the bypass of PC and TC3 than of DC, carrying a more suitable flow to perfuse the cerebral territory to be revascularized with respect to DC.

A common trend in all scenarios could be noticed with regard to the AChA, where all surgical solutions lowered the velocity, compared to the preoperative case. TC3 was the solution that maintained the highest flow, followed by PC and finally by DC with the least flow. This behaviour did not emerge from the velocity streamline maps (Figure 8), but was derived from the velocity isosurfaces for each alternative and PCoA diameter scenario (Figure 9).

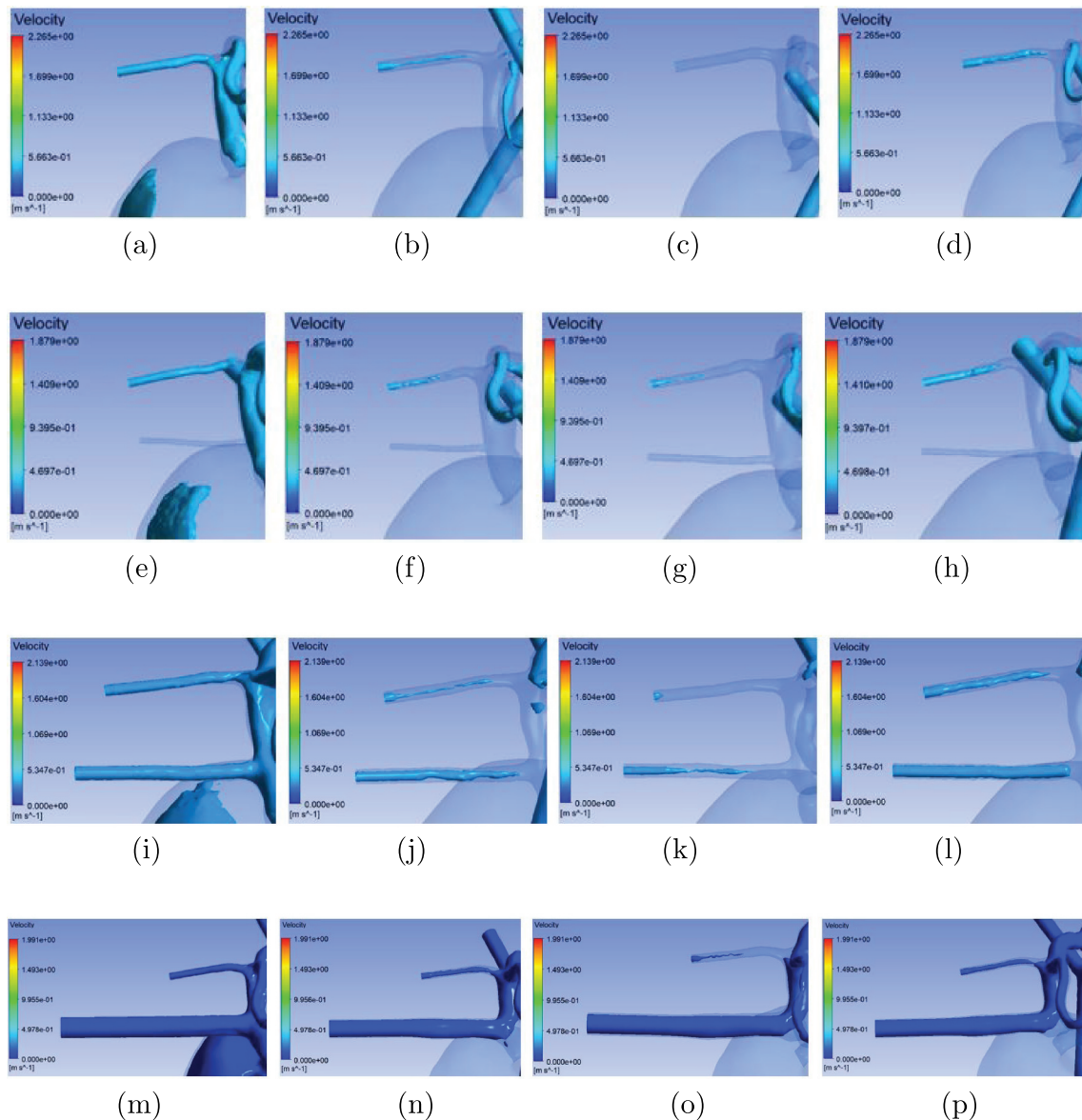


Figure 9. Right side view of velocity isosurfaces for alternative geometries: S_0 (a–d); S_m (e–h); S_a (i–l); S_M (m–p); pathological case (a,e,i,m); PC (b,f,j,n); DC (c,g,k,o); TC3 (d,h,l,p).

Focusing on the PCoA diameter, there were differences in the aneurysm and in the ophthalmic region as this diameter changes, especially in PC. In particular, a different number of lines from the C4 segment of the ICA reached the aneurysm and flowed into the OA, where they increased slightly in velocity: 3 lines in S_0 , 1 in S_m , 7 in S_a , and 1 in S_M (Figure 8 for S_a ; Online Supplementary Materials for S_0 , S_m and S_M). Although in S_m and S_M there was little flow to the OA, it should not be forgotten that it also came from the ECA and, therefore, the area supplied by the OA did not risk ischaemia. Anyway, flow reversal had not been simulated by this analysis. Considering the C4 segment of the ICA and the bifurcation between MCA and ACA, the flow increased with PC, attracted by the OA and the PCoA presence. In S_0 and S_m , there was recirculation at the level of the AChA, also present in S_a but much less as more flow reached the PCoA. With DC, recirculation was equally noticeable in S_0 at the level of the AChA, where the flow was interrupted and did not reach the C4 segment. By decreasing the resistance, in S_M the flow increased considerably compared to the other scenarios. In this scenario, the PCoA diameter was larger than that of MCA and ACA, unbalancing the directions of flow towards the PCoA at the expense of the other vessels. The ACA flow particularly suffered; compared to the preoperative case, it decreased a lot in S_M . In TC3, the flow in the C4 segment behaved in a similar way than in the other surgical solutions, with a recirculation at the level of the AChA in S_0 and an increasing trend in flow lines from S_m to S_M . Also the ACA was subject to the PCoA diameter variability: the blood flow rate that reached it was comparable to that in the preoperative situation only in S_0 and S_m and progressively decreased as the PCoA diameter increased. In S_M , becoming one of the predominant vessels, the PCoA was able to sequester more flow under all surgical solutions. Finally, MCA revealed a similar trend with all surgical solutions as the PCoA diameter increased.

3.4. Ranking of surgical alternatives

Our CFD results showed that TC3 is the best choice if only the aneurysm treatment is considered, as it excluded the diseased part from the network. PC blocked orthograde flow in the ICA and the retrograde flow from the bypass was minimal, placing this solution in second place. DC was found to be the worst option, as there was a direct flow from upstream (Wessels et al. 2021). Coherently, the pressure in the aneurysm and the OA was the highest with DC, followed by PC and TC3. The pressure in the aneurysm was even higher than in the preoperative case with DC, which remained the worst and most dangerous solution for the aneurysm. OA values exceeded preoperative case with DC, while they were lower with PC and equal to zero with TC3. However, the results regarding this perforating artery were not considered in the ranking as the OA can itself become a bypass by collecting blood from the ECA. This evolution is beyond the scope of this analysis. Considering WSS and velocity, the same ranking was identified based on the highest flow rate in the perforating artery (best TC3, intermediate PC and worst DC). Further items confirm this ranking; for instance, the bypass is more likely to fulfil cerebral demands with TC3 and PC, differently from DC.

This ranking was analysed by the neurosurgeon, who integrated the CFD outcomes with medical knowledge and skills. Despite being the most effective, TC3 is difficult to perform due to the positioning of clips, and because the distal clip must be placed close to the choroidal region, which increases the risk of ischaemia the smaller the PCoA is. As a matter of facts, TC3 is usually reserved for bleeding aneurysms. Therefore, the other alternatives were considered and, merging all aspects, PC resulted the best alternative both from the clinical and the CFD viewpoints. Indeed, it allows to heal the aneurysm without damaging the AChA.

While varying the PCoA diameter, no relevant differences were highlighted in the ranking of the surgical alternatives. In particular, the main points considered in the comparison between any surgical alternative and the preoperative case gave the same insights. Even if the values can vary with the PCoA diameter, the ordering of the phenomena and the resulting ranking were robust with respect to these diameter values and led to the same conclusions.

In this specific test case, the univocal ranking of the surgical alternatives while the PCoA diameter varied is an added value for the neurosurgeon, who does not have to make the decision once the surgery is started after observing the actual PCoA diameter. However, also in the presence of different rankings based on the unknown diameters of some vessels, the simulation results allow the neurosurgeon to choose the alternative based on the ranking for the specific scenario. Rather, in this case, the complexity of the decision is greater, and having a pool of already available scenarios among which to take one becomes even more important.

4. Discussion

The analysis of surgical options through CFD simulations is only of recent interest for neurosurgeons, as CFD was more often adopted to understand the evolution of IAs and the role of haemodynamics in their natural history, with the aim of predicting vessel rupture (Sforza et al. 2012; Ivanov et al. 2016). In this context, sophisticated studies accounting for blood flow pulsatility (Selimovic et al. 2010) or even the interaction between blood motion and wall structure (Bazilevs et al. 2010) are present in the literature, aiming at elucidating mechanisms of aneurysm progression that are not fully understood, yet.

Studies that report the evaluation of alternative surgical treatments through CFD analysis are still limited in the literature, and are mostly case studies with very important assumptions, such as steady state flows or boundary conditions, that are far from being patient-specific (Acevedo-Bolton et al. 2006; Russin et al. 2015; Xiang et al. 2015; Lawton et al. 2016; Vali et al. 2017; Bozzetto et al. 2022). Also, the impact of stents was assessed (Chong et al. 2014; Cosentino et al. 2015; Ouared et al. 2016; Berg et al. 2018), or advantages and disadvantages of newly proposed treatments were quantified (Sharifi et al. 2020). In these works, a risk score associated with each alternative enables the neurosurgeon to perform a preoperative assessment also based on quantitative haemodynamic information (Chung and Cebal 2015; Rayz et al. 2015; Walcott et al. 2016; Rashad et al. 2020). A recent work considered cerebral

aneurysms in particular (Chong et al. 2019), although it did not consider complex IAs.

However, recent discussions highlighted that the standardisation of pre-simulation procedures and post-processing of the results is needed in the context of CFD applied to complex IAs (Berg et al. 2019). Moreover, recent highly refined simulations suggested potential shortcomings in the approaches usually employed in CFD-based analyses of aneurysms (Valen-Sendstad and Steinman 2014). Our paper proposes a framework for IA surgery, in which neurosurgeon's expertise is supported by a quantitative interface that predicts the haemodynamics of any surgical treatment and compares it with the preoperative situation. We took inspiration from a previously developed case study (Bozzetto et al. 2022), and we extended methodology to meet standardisation and formalisation requirements.

The CFD analyses are based on patient-specific images. Therefore, they provide patient-specific suggestions, which is a fundamental requirement in the case of complex surgeries. At the same time, CFD does not require invasive measurements or additional examinations compared to those normally performed before surgery. This makes the framework effectively applicable to clinical practice. Also, the times to provide an answer conform to the usual schedule of IA elective surgeries.

Trusting the outcomes is a key point, which has been considered in the framework. On the one hand, a sensitivity analysis for the unknown secondary artery diameters is included by repeating the CFD simulations on alternative geometries. This gives information on the stability of the indication provided with respect to the unknown diameters, or formalises the need for additional measurements or assumptions. On the other hand, the provided guidelines guarantee intra- and inter-operator repeatability. Proof of this is given by the case study results, in which geometries and simulations were implemented by two independent operators and the results were found to be consistent and coherent. Anyway, operations require skill and attention to avoid operation-dependent differences; the most critical is the local smoothing step, where sculpt instruments are applied to the surface mesh at the user's discretion.

4.1. Limitations and future extensions

Patient-specific boundary conditions of flow and pressure were not considered in this work. In particular, due to the absence of specific boundary conditions for this patient (as is the case in most clinical cases), we assumed zero pressure at the outlets, while also ensuring the presence of adequate flow extensions. This is still a very common choice in the absence of patient-specific boundary conditions (Marzo et al. 2011; Chnafa et al. 2018). The other very common alternative is to use the Murray's law, based on the simplifying assumption of Poiseuille flow, which is not necessarily valid for all cerebral arteries; therefore, as with the zero-pressure assumption, the predicted flow rates and the other CFD outcomes would be affected by this assumption. In the future, our framework will be extended to analyse whether the cost of performing these measurements is offset by better haemodynamic results.

Also, to better quantify intracranial collateral flows distal to the aneurysm, we will analyse the impact of extending the considered volumes, e.g., by including the circle of Willis. This extension could also include hybrid models with full CFD combined with lumped parameter models.

The steady-state condition is also a limitation of this study. However, no patient-specific velocity waveforms were available for this patient, as is the case in most clinical cases. However, in formulating this assumption, we referred to several recent studies that used the steady-state assumption (Valen-Sendstad et al. 2013; Souche and Valen-Sendstad 2022). In particular, *et al.* Geers et al. (2014) demonstrated that steady-state simulations can accurately characterise the blood flow field in cerebral aneurysms. These studies allowed us to consider that the steady-state may also be acceptable for our study.

Fluid-structure interaction (FSI) was not considered in this study because of the computational cost and the need to assume parameters that cannot be measured directly (e.g., wall thickness and vessel material properties), which would lead to major uncertainties in the results. Looking at the recent literature on cerebral aneurysms, only a few works made use of FSI (Souche and Valen-Sendstad 2022; Bruneau et al. 2023), and these studies focused on the role of the wall itself in vascular remodelling. On the contrary, the aim of our study was to provide an assessment of changes in haemodynamic conditions, and from this perspective, the rigid wall assumption may be acceptable and has in fact been widely used in the past. In the future, and in the presence of available data, we will use FSI to show if and how the results can be more accurate by also modelling the effect of the wall.

Finally, the obtained risk scores could be further adjusted based on follow-up analyses, which would allow the neurosurgeon to verify to what extent the estimated outcomes correspond to those actually obtained.

5. Conclusion

This study proposed a CFD-based framework to evaluate alternative surgical interventions, and provided preliminary evidence on its effectiveness when applied to a complex IA. In particular, the proposed framework proved to be effective for planning surgeries of complex IAs, representing a flexible and reliable tool to support the surgeon's decision-making process, while also optimising the analysis time. The presented case study provided evidence that the framework delivers consistent and accurate results regardless of aneurysm complexity, by identifying a ranking of surgical alternatives based on reliable quantitative data.

Disclosure statement

No potential conflict of interest was reported by the author(s)

ORCID

Michela Bozzetto  <http://orcid.org/0000-0002-2045-5550>
 Andrea Remuzzi  <http://orcid.org/0000-0002-4301-8927>
 Luigi A. A. Lanterna  <http://orcid.org/0000-0001-9484-4834>
 Ettore Lanzarone  <http://orcid.org/0000-0001-8816-9086>

References

- Acevedo-Bolton G, Jou L-D, Dispensa BP, Lawton MT, Higashida RT, Martin AJ, Young WL, Saloner D. 2006. Estimating the hemodynamic impact of interventional treatments of aneurysms: numerical simulation with experimental validation: technical case report. *Neurosurgery*. 59(2): E429–E430. doi: [10.1227/01.NEU.0000223495.39240.9A](https://doi.org/10.1227/01.NEU.0000223495.39240.9A).
- Alnæs MS, Isaksen J, Mardal K-A, Romner B, Morgan MK, Ingebrigtsen T. 2007. Computation of hemodynamics in the circle of willis. *Stroke*. 38(9):2500–2505. doi: [10.1161/STROKEAHA.107.482471](https://doi.org/10.1161/STROKEAHA.107.482471).
- Andaluz N, Zuccarello M. 2011. Treatment strategies for complex intracranial aneurysms: review of a 12-year experience at the University of Cincinnati. *Skull Base*. 21(4):233. doi: [10.1055/s-0031-1280685](https://doi.org/10.1055/s-0031-1280685).
- Ashraf T, Panhwar Z, Habib S, Memon MA, Shamsi F, Arif J. 2010. Size of radial and ulnar artery in local population. *J Pak Med Assoc*. 60(10):817.
- Bazilevs Y, Hsu M-C, Zhang Y, Wang W, Kvamsdal T, Hentschel S, Isaksen J. 2010. Computational vascular fluid–structure interaction: methodology and application to cerebral aneurysms. *Biomech Model Mechanobiol*. 9(4):481–498. doi: [10.1007/s10237-010-0189-7](https://doi.org/10.1007/s10237-010-0189-7).
- Beecher J, Welch B. 2017. Surgical and endovascular management of patients with giant cerebral aneurysms. In: *Primer on cerebrovascular diseases*. Academic Press: Elsevier; p. 818–823. <https://www.sciencedirect.com/book/9780128030585/primer-on-cerebrovascular-diseases>.
- Berg P, Saalfeld S, Janiga G, Brina O, Cancelliere NM, Machi P, Pereira VM. 2018. Virtual stenting of intracranial aneurysms: a pilot study for the prediction of treatment success based on hemodynamic simulations. *Int J Artif Organs*. 41(11):698–705. doi: [10.1177/0391398818775521](https://doi.org/10.1177/0391398818775521).
- Berg P, Saalfeld S, Voß S, Beuing O, Janiga G. 2019. A review on the reliability of hemodynamic modeling in intracranial aneurysms: why computational fluid dynamics alone cannot solve the equation. *Neurosurg Focus*. 47(1):E15. doi: [10.3171/2019.4.FOCUS19181](https://doi.org/10.3171/2019.4.FOCUS19181).
- Botti L, Paliwal N, Conti P, Antiga L, Meng H. 2018. Modeling hemodynamics in intracranial aneurysms: comparing accuracy of CFD solvers based on finite element and finite volume schemes. *Int J Numer Method Biomed Eng*. 34(9):e3111. doi: [10.1002/cnm.3111](https://doi.org/10.1002/cnm.3111).
- Bozzetto M, Soliveri L, Volpi J, Remuzzi A, Barbieri A, Lanterna LAA, Lanzarone E. 2022. Computational fluid dynamic modeling of flow-altering surgical procedures: feasibility assessment on saccular aneurysm case study. *Comput Meth Biomech Biomed Eng Imaging Vis*. 11(4):1431–1437. doi: [10.1080/21681163.2022.2140310](https://doi.org/10.1080/21681163.2022.2140310).
- Bruneau DA, Valen-Sendstad K, Steinman DA. 2023. Onset and nature of flow-induced vibrations in cerebral aneurysms via fluid–structure interaction simulations. *Biomech Model Mechanobiol*. 22(3):761–771. doi: [10.1007/s10237-022-01679-x](https://doi.org/10.1007/s10237-022-01679-x).
- Chnafa C, Brina O, Pereira V, Steinman D. 2018. Better than nothing: a rational approach for minimizing the impact of outflow strategy on cerebrovascular simulations. *AJNR Am J Neuroradiol*. 39(2):337–343. doi: [10.3174/ajnr.A5484](https://doi.org/10.3174/ajnr.A5484).
- Chong B, Bendok B, Krishna C, Sattur M, Brown B, Tawk R, Miller D, Rangel-Castilla L, Babiker H, Frakes D, et al. 2019. A multicenter pilot study on the clinical utility of computational modeling for flow-diverter treatment planning. *Am J Neuroradiol*. 40(10):1759–1765. doi: [10.3174/ajnr.A6222](https://doi.org/10.3174/ajnr.A6222).
- Chong W, Zhang Y, Qian Y, Lai L, Parker G, Mitchell K. 2014. Computational hemodynamics analysis of intracranial aneurysms treated with flow diverters: correlation with clinical outcomes. *AJNR Am J Neuroradiol*. 35(1):136–142. doi: [10.3174/ajnr.A3790](https://doi.org/10.3174/ajnr.A3790).
- Chung B, Cebral JR. 2015. CFD for evaluation and treatment planning of aneurysms: review of proposed clinical uses and their challenges. *Ann Biomed Eng*. 43(1):122–138. doi: [10.1007/s10439-014-1093-6](https://doi.org/10.1007/s10439-014-1093-6).
- Cosentino D, Capelli C, Derrick G, Khambadkone S, Muthurangu V, Taylor AM, Schievano S. 2015. Patient-specific computational models to support interventional procedures: a case study of complex aortic re-coarctation. *EuroIntervention*. 11(6):669–672. doi: [10.4244/EIJY15M09_03](https://doi.org/10.4244/EIJY15M09_03).
- Geers A, Larrabide I, Morales H, Frangi A. 2014. Approximating hemodynamics of cerebral aneurysms with steady flow simulations. *J Biomech*. 47(1):178–185. doi: [10.1016/j.jbiomech.2013.09.033](https://doi.org/10.1016/j.jbiomech.2013.09.033).
- Grant EG, Benson CB, Moneta GL, Alexandrov AV, Baker JD, Bluth EI, Carroll BA, Eliasziw M, Gocke J, Hertzberg BS, et al. 2003. Carotid artery stenosis: gray-scale and doppler US diagnosis—society of radiologists in ultrasound consensus conference. *Radiology*. 229(2):340–346. doi: [10.1148/radiol.2292030516](https://doi.org/10.1148/radiol.2292030516).
- Hofman M, Jamróz T, Jakutowicz I, Jarski P, Masarczyk W, Niedbała M, Przybyłko N, Kocur D, Baron J. 2018. Endovascular treatment of complex intracranial aneurysms. *Polish J Radiol*. 83:109–114. doi: [10.5114/pjr.2018.74968](https://doi.org/10.5114/pjr.2018.74968).
- Ishihita Y, Tanikawa R, Noda K, Kubota H, Izumi N, Katsuno M, Ota N, Miyazaki T, Hashimoto M, Kimura T, et al. 2014. Universal extracranial-intracranial graft bypass for large or giant internal carotid aneurysms: techniques and results in 38 consecutive patients. *World Neurosurg*. 82(1–2):130–139. doi: [10.1016/j.wneu.2013.02.063](https://doi.org/10.1016/j.wneu.2013.02.063).
- Ivanov D, Dol A, Polienko A. 2016. Patient-specific hemodynamics and stress-strain state of cerebral aneurysms. *Acta Bioeng Biomech*. 18(2):9–17.
- Lawton MT, Abla AA, Rutledge WC, Benet A, Zador Z, Rayz VL, Saloner D, Halbach VV. 2016. Bypass surgery for the treatment of dolichoectatic basilar trunk aneurysms: a work in progress. *Neurosurgery*. 79(1):83–99. doi: [10.1227/NEU.0000000000001175](https://doi.org/10.1227/NEU.0000000000001175).
- Manini LAS. 2013. vmtk tutorials [Online]. <http://www.vmtk.org/tutorials>
- Marzo A, Singh P, Larrabide I, Radaelli A, Coley S, Gwilliam M, Wilkinson ID, Lawford P, Reymond P, Patel U, et al. 2011. Computational hemodynamics in cerebral aneurysms: the effects of modeled versus measured boundary conditions. *Ann Biomed Eng*. 39(2):884–896. doi: [10.1007/s10439-010-0187-z](https://doi.org/10.1007/s10439-010-0187-z).
- Müller J-D, Jitsumura M, Müller-Kronast N. 2012. Sensitivity of flow simulations in a cerebral aneurysm. *J Biomech*. 45(15):2539–2548. doi: [10.1016/j.jbiomech.2012.07.036](https://doi.org/10.1016/j.jbiomech.2012.07.036).
- Ouared R, Larrabide I, Brina O, Bouillot P, Erceg G, Yilmaz H, Lovblad K-O, Pereira VM. 2016. Computational fluid dynamics analysis of flow reduction induced by flow-diverting stents in intracranial aneurysms: a patient-unspecific hemodynamics change perspective. *J Neurointerv Surg*. 8(12):1288–1293. doi: [10.1136/neurintsurg-2015-012154](https://doi.org/10.1136/neurintsurg-2015-012154).
- Özdemir H, Artas H, Serhatlioglu S, Ogur E. 2006. Effects of overweight on luminal diameter, flow velocity and intima-media thickness of carotid arteries. *Diagn Intervent Radiol*. 12(3):142.
- Pekkan K, Whited B, Kanter K, Sharma S, De Zelicourt D, Sundareswaran K, Frakes D, Rossignac J, Yoganathan AP. 2008. Patient-specific surgical planning and hemodynamic computational fluid dynamics optimization through free-form haptic anatomy editing tool (surgem). *Med Biol Eng Comput*. 46(11):1139–1152. doi: [10.1007/s11517-008-0377-0](https://doi.org/10.1007/s11517-008-0377-0).
- Pescatori L, Grasso G, Tropeano MP, Torregrossa F, Santoro G, Ciappetta P. 2022. Management of complex cerebral aneurysms. *World Neurosurg*. 159:266–275. doi: [10.1016/j.wneu.2021.11.077](https://doi.org/10.1016/j.wneu.2021.11.077).
- Rashad S, Saqr KM, Fujimura M, Niizuma K, Tominaga T. 2020. The hemodynamic complexities underlying transient ischemic attacks in early-stage Moyamoya disease: an exploratory CFD study. *Sci Rep*. 10(1):1–13. doi: [10.1038/s41598-020-60683-2](https://doi.org/10.1038/s41598-020-60683-2).
- Rayz V, Abla A, Boussel L, Leach J, Acevedo-Bolton G, Saloner D, Lawton M. 2015. Computational modeling of flow-altering surgeries in basilar aneurysms. *Ann Biomed Eng*. 43(5):1210–1222. doi: [10.1007/s10439-014-1170-x](https://doi.org/10.1007/s10439-014-1170-x).
- Russin J, Babiker H, Ryan J, Rangel-Castilla L, Frakes D, Nakaji P. 2015. Computational fluid dynamics to evaluate the management of a giant internal carotid artery aneurysm. *World Neurosurg*. 83(6):1057–1065. doi: [10.1016/j.wneu.2014.12.038](https://doi.org/10.1016/j.wneu.2014.12.038).
- Rutledge C, Baranoski JF, Catapano JS, Lawton MT, Spetzler RF. 2022. Microsurgical treatment of cerebral aneurysms. *World Neurosurg*. 159:250–258. doi: [10.1016/j.wneu.2021.12.079](https://doi.org/10.1016/j.wneu.2021.12.079).
- Saeki N, Rhoton AL. 1977. Microsurgical anatomy of the upper basilar artery and the posterior circle of Willis. *J Neurosurg*. 46(5):563–578. doi: [10.3171/jns.1977.46.5.0563](https://doi.org/10.3171/jns.1977.46.5.0563).
- Selimovic A, Penrose J, Bogunovic H, Villa-Uriol M-C, Holzapfel GA, Ventikos Y, and Watton PN. 2010. A computational framework to explore the role of pulsatile haemodynamics on cerebral aneurysm development for patient-specific arterial geometries. 6th World Congress of Biomechanics (WCB 2010); In Conjunction with 14th International Conference on Biomedical Engineering (ICBME) and 5th Asia Pacific Conference on Biomechanics (APBiomech); August 1-6; Singapore, Republic of Singapore. Springer, 759–762.

- Sforza DM, Putman CM, Cebal JR. 2012. Computational fluid dynamics in brain aneurysms. *Int J Numer Method Biomed Eng.* 28(6–7):801–808. doi: [10.1002/cnm.1481](https://doi.org/10.1002/cnm.1481).
- Sharifi A, Deyranlou A, Moghadam MC, Niazmand H. 2020. Numerical simulation of blood flow in intracranial aneurysms treated by endovascular woven endobridge technique. *Int J Mod Phys C.* 31(5):2050073. doi: [10.1142/S0129183120500734](https://doi.org/10.1142/S0129183120500734).
- Souche A, Valen-Sendstad K. 2022. High-fidelity fluid structure interaction simulations of turbulent-like aneurysm flows reveals high-frequency narrowband wall vibrations: a stimulus of mechanobiological relevance? *J Biomech.* 145:111369. doi: [10.1016/j.jbiomech.2022.111369](https://doi.org/10.1016/j.jbiomech.2022.111369).
- Valen-Sendstad K, Mardal K-A, Steinman DA. 2013. High-resolution cfd detects high-frequency velocity fluctuations in bifurcation, but not sidewall, aneurysms. *J Biomech.* 46(2):402–407. doi: [10.1016/j.jbiomech.2012.10.042](https://doi.org/10.1016/j.jbiomech.2012.10.042).
- Valen-Sendstad K, Steinman D. 2014. Mind the gap: impact of computational fluid dynamics solution strategy on prediction of intracranial aneurysm hemodynamics and rupture status indicators. *AJNR Am J Neuroradiol.* 35(3):536–543. doi: [10.3174/ajnr.A3793](https://doi.org/10.3174/ajnr.A3793).
- Vali A, Abila AA, Lawton MT, Saloner D, Rayz VL. 2017. Computational fluid dynamics modeling of contrast transport in basilar aneurysms following flow-altering surgeries. *J Biomech.* 50:195–201. doi: [10.1016/j.jbiomech.2016.11.028](https://doi.org/10.1016/j.jbiomech.2016.11.028).
- Walcott BP, Reinshagen C, Stapleton CJ, Choudhri O, Rayz V, Saloner D, Lawton MT. 2016. Predictive modeling and in vivo assessment of cerebral blood flow in the management of complex cerebral aneurysms. *J Cereb Blood Flow Metab.* 36(6):998–1003. doi: [10.1177/0271678X16641125](https://doi.org/10.1177/0271678X16641125).
- Wei ZA, Huddleston C, Trusty PM, Singh-Gryzbon S, Fogel MA, Veneziani A, Yoganathan AP. 2019. Analysis of inlet velocity profiles in numerical assessment of Fontan hemodynamics. *Ann Biomed Eng.* 47(11):2258–2270. doi: [10.1007/s10439-019-02307-z](https://doi.org/10.1007/s10439-019-02307-z).
- Wessels L, Hecht N, Faust K, Schneider U, Czabanka M, Vajkoczy P. 2021. Complete or partial parent artery sacrifice: effect of vessel-occlusion strategies on complete obliteration of complex aneurysms. *World Neurosurg.* 147:e282–e292. doi: [10.1016/j.wneu.2020.12.050](https://doi.org/10.1016/j.wneu.2020.12.050).
- Xiang J, Damiano RJ, Lin N, Snyder KV, Siddiqui AH, Levy EI, Meng H. 2015. High-fidelity virtual stenting: modeling of flow diverter deployment for hemodynamic characterization of complex intracranial aneurysms. *J Neurosurg.* 123(4):832–840. doi: [10.3171/2014.11.JNS14497](https://doi.org/10.3171/2014.11.JNS14497).
- Zhao M, Amin-Hanjani S, Ruland S, Curcio A, Ostergren L, Charbel F. 2007. Regional cerebral blood flow using quantitative MR angiography. *AJNR Am J Neuroradiol.* 28(8):1470–1473. doi: [10.3174/ajnr.A0582](https://doi.org/10.3174/ajnr.A0582).
- Zhao J, Lin H, Summers R, Yang M, Cousins BG, Tsui J. 2018. Current treatment strategies for intracranial aneurysms: an overview. *Angiology.* 69(1):17–30. doi: [10.1177/0003319717700503](https://doi.org/10.1177/0003319717700503).